



This is a repository copy of *A novel oblique impact model for unified particle breakage master curve*.

White Rose Research Online URL for this paper:

<https://eprints.whiterose.ac.uk/197247/>

Version: Accepted Version

Article:

Wang, L.G., Litster, J.D. and Smith, R.M. orcid.org/0000-0003-2340-0042 (2023) A novel oblique impact model for unified particle breakage master curve. *Chemical Engineering Science*, 268. 118397. ISSN 0009-2509

<https://doi.org/10.1016/j.ces.2022.118397>

Article available under the terms of the CC-BY-NC-ND licence (<https://creativecommons.org/licenses/by-nc-nd/4.0/>).

Reuse

This article is distributed under the terms of the Creative Commons Attribution-NonCommercial-NoDerivs (CC BY-NC-ND) licence. This licence only allows you to download this work and share it with others as long as you credit the authors, but you can't change the article in any way or use it commercially. More information and the full terms of the licence here: <https://creativecommons.org/licenses/>

Takedown

If you consider content in White Rose Research Online to be in breach of UK law, please notify us by emailing eprints@whiterose.ac.uk including the URL of the record and the reason for the withdrawal request.



eprints@whiterose.ac.uk
<https://eprints.whiterose.ac.uk/>

A Novel Oblique Impact Model for Unified Particle Breakage Master Curve

Li Ge Wang^{1,2}, Rachel Smith^{2*}, James D. Litster²

¹Process Systems Enterprise, Hammersmith, London, UK

²Department of Chemical and Biological Engineering, University of Sheffield, UK

Email: Rachel.Smith@sheffield.ac.uk

Abstract

Many experimental and numerical studies have been performed on the impact breakage of particulate solids, leading to a variety of impact breakage models developed to predict breakage probability. Ideally, impact breakage models would be mechanistic in nature, mathematically simple and inclusive of critical breakage parameters. In this paper, a critical review of the most widely used impact breakage models is presented, with the conclusion that the majority of existing breakage models inadequately predict breakage probability under oblique impact. In this work, a novel oblique impact model is proposed where the effect of impact angle is considered by the equivalent velocity. A breakage database compiled from the literature is deployed to interrogate the validity of the proposed model across a variety of oblique impact circumstances. In this way, the new oblique impact model is shown to provide excellent predictions of breakage probability, requiring only one set of fitting parameters under various impact angles. The unique feature of this oblique impact model is not necessarily required to be used with any specific normal impact breakage models, but can instead be universally applied with any of the assessed normal impact breakage models to establish unified breakage master curves for any oblique impact.

Keywords: Oblique impact model; Breakage model assessment; Unified master curve; Impact angle; Equivalent velocity

25 **1 Introduction**

26 The prediction of particle impact breakage has been a longstanding topic across many
27 engineering fields. Particle breakage is widely observed in numerous phenomena such as rock
28 falls in geotechnical engineering (Ye et al., 2021), ball mill in mineral engineering (De Carvalho
29 and Tavares, 2013), catalyst attrition in chemical engineering (Boerefijn et al., 2000), impact
30 mill in pharmaceutical engineering (Li et al., 2020). Central to a fundamental understanding
31 of particle impact breakage is the identification of critical breakage parameters, which can
32 then be incorporated and formulated in mathematical or theoretical models. These breakage
33 parameters can be briefly divided into particle (i.e. material) parameters and impact (i.e.
34 process) parameters. The particle parameters include but are not limited to particle size (Shi,
35 2016), particle structure (Ge et al., 2019; Wang et al., 2015), moisture content (Mueller et al.,
36 2011) and mechanical properties, i.e. hardness and fracture toughness (Wang et al., 2021a).
37 Larger particles are more prone to impact breakage than smaller particle due to higher crack
38 density in larger particles (Shi, 2016).

39 The process parameters are mainly composed of impact velocity (Evans et al., 1978) either
40 impact energy (Tavares, 2004), impact angle (Portnikov et al., 2018; Wang et al., 2021a) and
41 impact frequency (Bwalya and Chimwani, 2020; Rozenblat et al., 2013; Tavares, 2009;
42 Zhang et al., 2022). Impact velocity is typically recognized as the most influential
43 impact parameter in particle breakage. Increasing the impact velocity transitions the
44 breakage mode from chipping to fragmentation (Mueller et al., 2014; Subero and Ghadiri,
45 2001; Wang, 2016). Damage accumulation or strength degradation occurs in the majority of

46
47
48
49
50
51
52
53
54
55

56 comminution systems due to multiple impact loading events, i.e. impact frequency. A
57 distinctive feature of impact frequency is that particles undergoing lower impact velocity and
58 multiple impacts have the same consequence of particles with single impact with higher
59 impact velocity (Wang et al., 2021c). In other words, the breakage probability will be
60 increased with increasing impact number under identical impact velocities.

61 Impact angle is another critical impact parameter in particle breakage, which is defined by the
62 acute angle between the particle impact direction and the impact target (Wang et al., 2021a).
63 It has been shown that impact angle becomes increasingly important with increasing impact
64 velocity (Cheong et al., 2003). Whilst the breakage probability is defined by an experimental
65 means, the damage ratio, i.e. the extent of broken bonds, is usually adopted by DEM
66 simulation of oblique impact (Chen et al., 2022; Moreno et al., 2003; Wang et al., 2022). DEM
67 simulations of agglomerate breakage under oblique impact indicate the damage ratio is
68 predominantly dependent on the normal velocity, whilst tangential velocity has little effect.
69 However, the size distribution of fragments was affected by the impact angle. Note that the
70 above conclusion is only applicable to spherical agglomerates under relatively low impact
71 velocity (Moreno et al., 2003). By that time, the DEM study of particle shape was only
72 intended as spherical and the spectrum of impact velocity is varied from 1 m/s to 4.8 m/s. The
73 effect of impact angle for non-spherical particles beyond the relatively low impact velocity is
74 not investigated in their study. For non-spherical agglomerates, the damage model and
75 degree depends on not only impact velocity, impact angle but also impact orientation (Liu et
76 al., 2010). This is because of the synergic effect of impact orientation and impact angle
77 resulting in varying contact modes upon impact. The amount of debris produced was shown
78 to be highly sensitive to the impact location for non-spherical agglomerates (Liu et al., 2010).
79 It is important to highlight the notable difference of breakage evaluation by breakage ratio
80 from experiments compared to damage ratio from DEM simulations. In experiments,
81 breakage ratio is traditionally quantified by the ratio of debris mass to the total mass of
82 mother particles; The damage ratio is calculated based on the amount of broken bonds in the
83 particle assembly. Due to this disparity, very few literature work made direct comparison of
84 the breakage results between experimental and DEM simulations.

85 A series of impact breakage models have been developed to account for breakage parameters
86 such as particle size, impact velocity or energy and impact number. In particular, a breakage

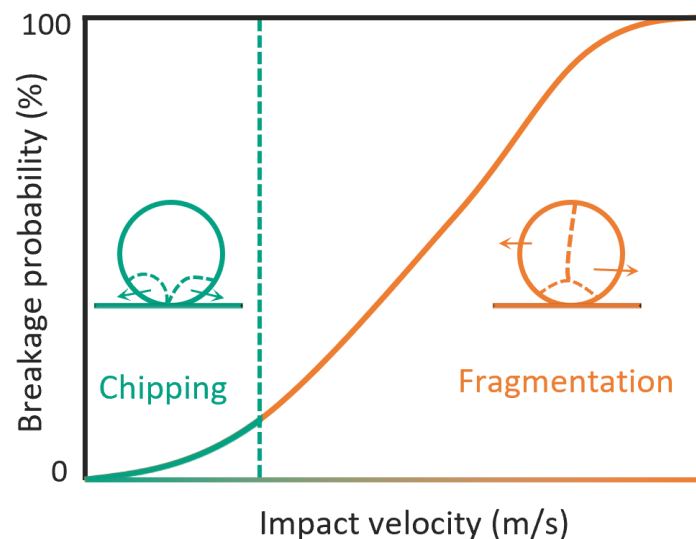
87 model developed by Vogel and Peukert is able to quantify the breakage probability of various
88 particles through the use of a breakage master curve (Vogel and Peukert, 2003). The breakage
89 master curve for five polymers, limestone and glass spheres with different sizes was
90 successfully constructed with two model parameters. The first model parameter f_{Mat} defines
91 the resistance of the particle to external stresses, whilst the second model parameter $W_{m,min}$
92 denotes the mass-specific threshold energy for particle to break. Whilst the Vogel and Puekert
93 model was initially developed to predict breakage probability, the modification of its form
94 was enabled to describe the breakage index t_{10} (%) concerning the particle size distribution.
95 The modified breakage index t_{10} has the advantage of only requiring one set of model
96 parameters, with particle size and breakage properties incorporated explicitly. Despite its
97 success in establishing a unified master curve for impact velocity and impact number, the
98 Vogel and Peukert model falls short of constructing a master curve for impact angle. However,
99 recent studies have shown increasing amount of research regarding oblique impact breakage
100 (Cavalcanti et al., 2021; Wang et al., 2021a).

101 The principal objectives of this paper are two-fold: (a) to provide a critical review and
102 assessment of existing impact breakage models relevant to the oblique impact, and (b) to
103 demonstrate the universality of a novel oblique impact model with the chosen set of literature
104 database. The former part serves to scrutinize assumptions, expression and application
105 between existing particle breakage models. The difference between chipping and
106 fragmentation models is clarified and the significance of impact angle is highlighted,
107 quantification of which is lacking in the literature. The summary of existing breakage models
108 identifies the detriment of ignoring impact angle, as its importance has been experimentally
109 and computationally observed but rarely considered in a theoretically based model. A unique
110 feature of the novel oblique impact model is that it is not necessarily appended to any specific
111 normal impact breakage models. Instead, it can be universally used with all the assessed
112 breakage models assessed in this paper, to establish unified breakage master curves subject
113 to various impact angles. As the majority of existing breakage models are inadequate to
114 describe oblique impact conditions, and oblique impact is a substantial contribution to milling
115 processes, this is a substantial contribution to the particle breakage field.

116 **2 Overview of impact breakage models**

117 **2.1 Impact breakage models**

118 Prior to the overview of impact breakage models, it is noteworthy to distinguish breakage
119 patterns, i.e. chipping and fragmentation, as a function of impact velocity. Chipping is also
120 termed as surface breakage, whilst fragmentation is termed as body breakage by other
121 researchers (Kotzur et al., 2018; Tavares, 2021). The transition from chipping to
122 fragmentation with increasing impact velocity is illustrated in Figure 1. Under low impact
123 velocity, the particle will undergo loss of debris, but still sustain its entity. Above a certain
124 threshold impact velocity, the particle undergoes fragmentation which was simulated using
125 an elasto-dynamic finite element method (Andrews and Kim, 1999). The particle will be
126 broken to several pieces of fragments as the threshold impact velocity is surpassed. This
127 results from the propagation of median and radial cracks throughout the entire body of
128 particles (Kotzur et al., 2018). There exists several ways to define breakage probability, but
129 the calculation of mass percentage of particles lower than the initial particle size is usually
130 adopted (Antonyuk et al., 2006). As a result, the breakage probability will be defined as 100%
131 when the size of impacted particle falls below the lower limit of the initial size distribution.
132 There are no mechanistic-based methods to distinguish the impact velocity threshold for the
133 breakage pattern transition. However, as a rule of thumb, chipping can be defined with less
134 than 10% mass loss, beyond which fragmentation occurs with increased impact velocity
135 (Cavalcanti et al., 2021). As such, the threshold of breakage probability for chipping is 46%
136 with equivalent breakage size, converted from 10 % mass loss of initial particles.



137

138 Figure 1 Breakage pattern as a function of impact velocity (modified from Wang et al.,

139

2021b)

140 Over the last decades, there have been significant efforts in developing particle breakage
141 models to elaborate the influence of critical breakage parameters on breakage probability.
142 Previous studies on the breakage models mainly focused on the normal impact. As a
143 consequence, most of the breakage models are initially applied to normal impact, and only
144 the normal component velocity is considered under oblique impact.

145 The chipping model can be expressed as a function of impact velocity using power functions.
146 The fragmentation model is usually developed based on Weibull distribution (A. D. Salman et
147 al., 2003) or logistic distribution (Petukhov and Kalman, 2004) or log-normal distribution
148 (Tavares and King, 1998). Comprehensive assessment of impact breakage models has been
149 carried out by several researchers (Rozenblat et al., 2012; Wang et al., 2021a, 2021b).
150 Rozenblat et al. shortlisted 6 breakage models including Petukhov and Kalman model
151 (Petukhov and Kalman, 2004), Salman et al. model (A. Salman et al., 2003), Pocock et al. model
152 (Pocock et al., 1998), Duo et al. model (Duo et al., 1996), Boerefijn et al. model (Boerefijn et
153 al., 2000) and Cleaver and Ghadiri model (Cleaver et al., 1993). Only the first three models are
154 used for model assessment of fragmentation, as the last three models are intended for
155 chipping. Whilst these three fragmentation models exhibit nearly the same fitting quality
156 against the experimental data, model simplicity and statistical meaning of model parameters
157 are the basis in the appropriate model selection (Rozenblat et al., 2012). An assessment of
158 breakage models to predict the particle size distribution was performed in an impact pin mill,
159 in the context of a population balance model (Wang et al., 2021b). These assessed models
160 include the Weichert model, Pocock model, Vogel and Peukert model, Antonyuk et al. model
161 and Portnikov-Kalman model (Wang et al., 2021b). These five models are shown to give close
162 agreement with particle size distribution in the impact pin mill. In particular, the logistic
163 distribution of the Portnikov-Kalman model was identified as the strongest performer from a
164 statistical performance viewpoint. Despite all these advancements, consideration of impact
165 angle in either the particle scale or the process scale is insufficient. In view of the focal point
166 in the present work, only the breakage models relevant to oblique impact will be presented
167 for brevity.

168 A Weibull-based breakage probability was developed by Weichert as a function of mass-
169 specific energy and it gives:

$$P = 1 - \exp(-cd^2W_m^z) \quad (1)$$

170 where $W_m = 0.5 * v^2$ is the mass-specific energy where v denotes the impact velocity; d is the
171 particle diameter; c and z are fitting parameters.

172 Another Weibull-based function to describe the breakage probability is given (A. Salman et
173 al., 2003)

$$P = 1 - \exp(-(v/a)^b) \quad (2)$$

174 where v is the impact velocity whereas a and b are the fitting parameters.

175 The difference between Weichert model and Salman et al. model lies in the expression of
176 mass-specific energy and impact velocity respectively.

177 A lognormal distribution function can be used to describe a breakage probability on the basis
178 of specific fracture energy (Pocock et al., 1998):

$$P_E = \frac{1}{2} \left[1 + \operatorname{erf} \left(\frac{\ln W_{m,kin} - E_{50,i}}{\sqrt{2}\sigma} \right) \right] \quad (3)$$

179 where P_E denotes the breakage probability as a function of specific energy; $W_{m,kin}$, $E_{50,i}$ and
180 σ denote the mass specific energy, median mass specific energy and standard deviation of
181 the specific energy.

182 A modified form of normal impact breakage models is developed to consider the impact angle
183 and it gives (Portnikov et al., 2018):

$$P = 1 - \frac{1}{1 + (v/v_{50})^b} \quad (4)$$

184 where P is the breakage probability, selection function; v_{50} denotes the median impact
185 velocity resulting in 50% of particle impact breakage. b is the logistic parameter to describe
186 scattering of breakage data.

187 The relationship between impact angle θ and the median impact velocity v_{50} gives (Portnikov
188 et al., 2018):

$$v_{50} = A_v \exp(-x/d_0) [4.4 \exp(-\theta/18.1) + 1] \quad (5)$$

189 where A_v and d_0 are fitting parameters; x is the particle size.

190 Eq. (5) indicates that v_{50} is varied with regard to impact angle θ and increases with the
191 decrease of impact angle.

192 A chipping model, which is called surface breakage in the original source (Cavalcanti et al.,
193 2021) was proposed based on DEM simulation of oblique collision and it gives:

$$\tilde{\varepsilon} = 100 k d e E_{loss} \quad (6)$$

194 where k denotes the Hertzian stiffness of the contact target; d is not clearly specified in the
195 original source; e denotes the fraction of loss energy in a collision event; E_{loss} is the mass-
196 specific collision energy, calculated using DEM. The surface breakage is also called attrition
197 and abrasion in the literature (Tavares, 2009), indicating a small amount of breakage due to
198 debris loss under low impact velocity. Particle undergoing surface breakage keeps its size
199 relatively unchanged along with fine progeny produced as the mass loss.

200 The mass-based energy loss E_{loss} is further expressed by

$$E_{loss} = \frac{E'_{loss}}{m_p} \quad (7)$$

201 where E'_{loss} denotes the total energy loss in the collision, calculated from DEM and m_p is the
202 mass of a pellet.

203 When oblique impact occurs with an impact angle θ , the total energy loss gives

$$E'_{loss} = W_m (3 * 10^{-7} \theta^3 - 1.3 * 10^{-4} \theta^2 + 1.7 * 10^{-2} \theta) \quad (8)$$

204 where W_m is the specific impact energy, equal to $v^2/2$. Eq. (8) indicates the total energy loss
205 abides by a polynomial distribution with respect to the impact angle θ .

206 Although Eqs. (5) and (8) take into account the impact angle, a main challenge remains
207 whether a master curve can be established with a single set of fitting parameters regarding
208 impact angle. Vogel and Peukert (Vogel and Peukert, 2003) developed a master curve of
209 breakage probability by unifying several parameters in a single predictive line as:

$$P_x = 1 - \exp\{-f_{Mat} x n (W_{m,kin} - W_{m,min})\} \quad (9)$$

210 where P_x denotes the breakage probability; f_{Mat} denotes the resistance of the particle
 211 against the external load; $W_{m,kin}$ is mass-specific kinetic energy; x and n are particle size and
 212 impact number. $W_{m,min}$ represents the mass-specific threshold energy for particle to break.

213 A generic form of chipping models is summarized (Wang et al., 2021a)

$$P_x = \frac{\rho^a v^b x^c H^d}{k_c^e} \quad (10)$$

214 where ρ and x are particle density and particle size; v is the impact velocity usually spanning
 215 in relatively low regime. H and k_c are the particle hardness and fracture toughness.

216 a , b , c , d , and e are the exponent of the abovementioned parameters. The existing chipping
 217 models (Evans et al., 1978; Evans and Wilshaw, 1976; Ghadiri and Zhang, 2002) are rooted
 218 from the same mechanical foundation, i.e. indentation fracture process. The notable
 219 difference within these chipping models is the varying velocity exponent b . As the impact
 220 velocity is the most influential parameter, Eq. (10) can be further simplified when the
 221 mechanical properties are not known:

$$P_x = m * v^b \quad (11)$$

222 where $m = \frac{\rho^a x^c H^d}{k_c^e}$ is treated as a single lumping parameter.

223 It has been nearly two decades for Vogel and Peukert model to construct a unified master
 224 curve including particle size, impact energy, impact frequency. This model has been
 225 successfully used with a wide application into materials like limestone, glass spheres, and
 226 polymethyl methacrylate (PMMA). However, the impact angle as another critical breakage
 227 parameter is excluded in this model. To address this challenge, a novel oblique impact model
 228 is thus developed with an attempt to establish a unified master curve for oblique impact
 229 breakage. A summary of critical parameters considered in the existing normal breakage
 230 models is shown in Table 1.

231 Table 1 Critical parameters considered by existing normal impact breakage models (Modified from Wang et al., 2021b)

Number	Breakage model	Mathematical form	Particle size	Mechanical property	Impact velocity	Impact frequency	Impact angle
1	Pocock et al., 1998	Lognormal	Yes	Yes	Yes	Yes	No
2	Salman et al., 2003	Weibull	No	No	Yes	No	No
3	Vogel and Peukert, 2003	Weibull	Yes	Yes	Yes	Yes	No
4	Portnikov-Kalman, 2018	Logistic	Yes	Yes	Yes	Yes	Yes
5	Wang et al., 2021a	Power	Yes	Yes	Yes	No	Yes

232

233 2.2 A novel oblique impact model

234 Appreciable progress of oblique impact breakage has been made with concluding remarks
235 that normal component velocity is dominant in particle breakage (Salman et al., 1995; Wang,
236 2016). However, in most cases, the understanding gained is based on experimental breakage
237 tests or computational DEM simulations. A mechanistic-based breakage model subject to
238 oblique impact is not yet available. Recent work for oblique impact model development was
239 performed, where the contribution of tangential velocity component is justified (Wang et al.,
240 2021a). The main equations of the developed oblique impact model are briefly recalled for
241 the sake of completeness. Further details about the analytical formulations can be found in
242 the original publication (Wang et al., 2021a).

243 The normal component v_n and tangential component v_t of an impact velocity v with impact
244 angle θ can be given by

$$v_n = v \sin \theta \quad (12)$$

$$v_t = v \cos \theta \quad (13)$$

245 Regardless of impact angle θ , the resultant impact velocity is hereby given by

$$v = v \sqrt{\sin^2 \theta + \cos^2 \theta} \quad (14)$$

246 Accordingly, the normal impact force F_n and the tangential impact force F_t are expected to
247 arise from the normal component velocity v_n and tangential component velocity v_t .

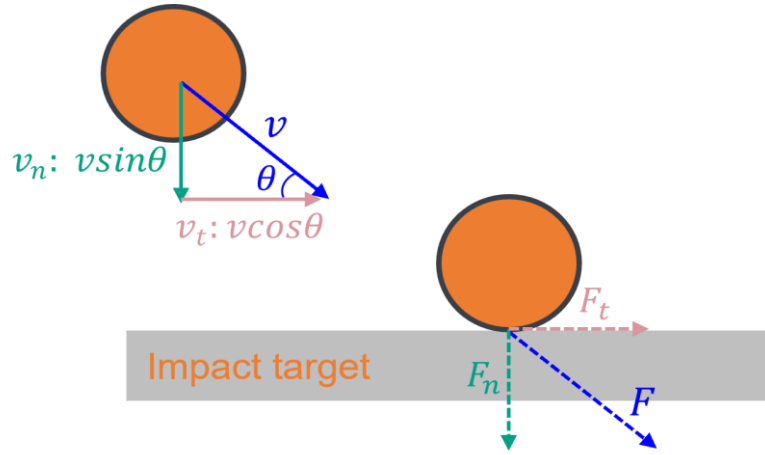
248 As a result, the resultant impact force F is given by

$$F = \sqrt{F_n^2 + F_t^2} \quad (15)$$

249 It is well known that the breakage induced by F_n and F_t are differing despite the same input
250 value and time characteristics. Hence, it is more appropriate to propose an equivalent impact
251 force F_e where the breakage caused by F_n can be comparable to that caused by F_t and it gives

$$F_e = \sqrt{F_n^2 + \alpha^2 F_t^2} \quad (16)$$

252 where α is the fitting parameter to correlate the breakage caused by tangential force F_t . The
 253 schematic of impact velocity and impact force with normal and tangential components is
 254 shown in Figure 2.



255

256 Figure 2 Schematic of impact velocity and impact force with normal and tangential
 257 components under oblique impact

258 Furthermore, the activation of tangential impact force F_t is relied on contact friction and
 259 more specifically is determined by the dynamic friction coefficient between the particle and
 260 the impact target, i.e. $F_t \leq \mu F_n$. Similar to the equivalent impact force F_e , an effective
 261 tangential velocity associate with the effective tangential impact force F_t can be formulated
 262 by

$$v_{te} = \mu v \sin \theta \cos \theta \quad (17)$$

263 Analogue to Eq. (17), the equivalent velocity v_{eq} can hereby be defined as below:

$$v_{eq} = \sqrt{v_n^2 + \alpha^2 v_{te}^2} \quad (18)$$

264 Substituting Eq. (17) into Eq. (18), it evolves

$$v_{eq} = v \sqrt{\sin^2 \theta + \psi^2 \sin^2 \theta \cos^2 \theta} \quad (19)$$

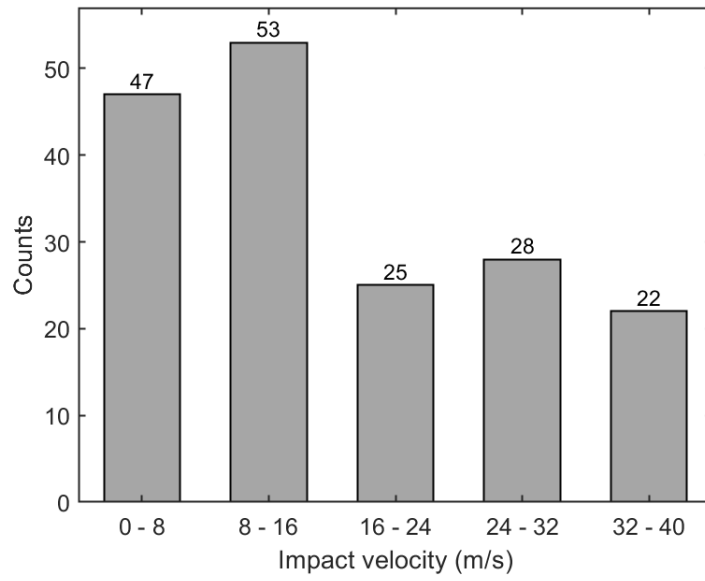
265 Comparing Eq. (19) with Eqs. (12) and (14), it can be found that equivalent velocity falls in
 266 between the normal velocity and the impact velocity.

267 The lumped parameter $\psi = \alpha\mu$ reflects the combination of frictional behaviour and the
268 correlation with tangential velocity. The equivalent velocity in Eq. (19) can be appended to
269 any existing breakage models. A simple treatment is to replace the normal velocity with
270 equivalent velocity under oblique impact conditions. However, the success of Eq. (19) has
271 only been established with a limited amount of breakage models and breakage database
272 (Wang et al., 2021a). This study is to pursue a comprehensive assessment of the proposed
273 oblique impact model in a wide spectrum of breakage database from the literature.

274 **3 Literature database**

275 A wide variety of literature database was collected and used for oblique model assessment
276 from an extensive scope of relevant scholarly work. The database covers 5 types of particles
277 and 175 datapoints with the impact angle spanning from 10° to 90° , which can be found in
278 the appended link of Excel file. The distribution of the collective data of impact angles is
279 plotted in Figure 3. In Figure 3a, the impact velocity is varied from 1.2 m/s to 40 m/s and the
280 impact velocity between 32 m/s and 40 m/s accounts for the least amount amongst the five
281 bin size regimes. In Figure 3b, the impact angles are categorized into 5 bin sizes with the
282 incremental value of 16° . The impact angles between 74° and 90° accounts for the largest
283 fraction whilst the impact angles between 58° and 74° is least represented. The detailed
284 features of test conditions in the breakage database are reported in the Appendix. In Figure
285 3c, the lower breakage probabilities from zero to 0.2, 0.4-0.6 have the largest proportion of
286 test data. The breakage probabilities between 0.8 and 1.0 have the minimum number of 19
287 test points, which corresponds to the least amount of impact velocity ranging 32 m/s to 40
288 m/s in Figure 3a.

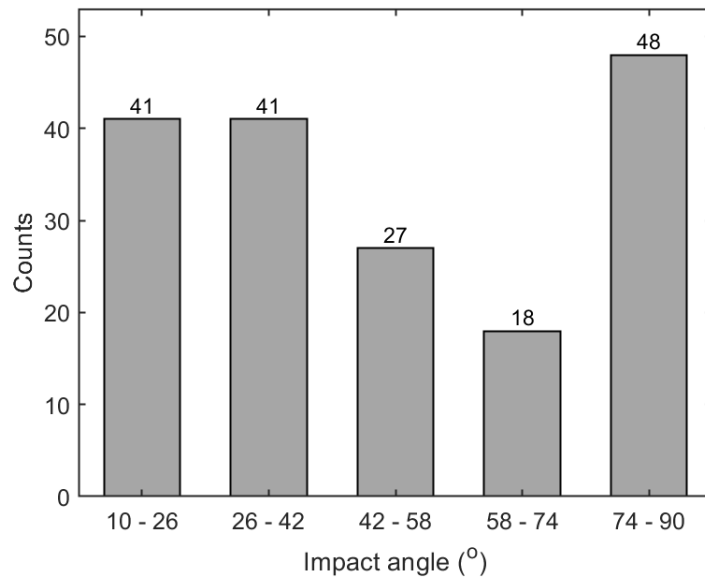
289 It is clear that the combined database spans a wide range of key features, and therefore
290 provides a robust benchmark for the oblique impact model assessment. It is encouraged that
291 future data be gathered in under-represented data classifications. For example, the impact
292 breakage tests under the impact angles 58° - 74° are encouraged for future work.



293

294

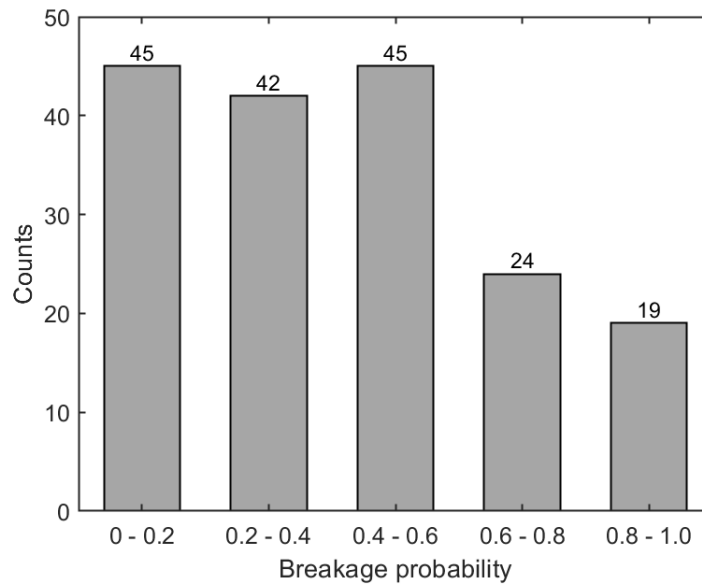
(a)



295

296

(b)



297

298

(c)

299

Figure 3 Histogram distribution of key factors in the test database (a) Range of impact

300

velocity (b) Range of impact angle (c) Range of breakage probability

301

302 3.1 Experimental database

303

The experimental database is composed of breakage results from three publications (Jägers

304

et al., 2021; Portnikov et al., 2018; Salman et al., 2002). The test materials under oblique

305

impact include 2.36-3.35 mm salt particles (Portnikov et al., 2018), 3.2 mm fertiliser particles

306

(Salman et al., 2002), and 15 mm wood pellet (Jägers et al., 2021). Note that the breakage

307

probability in the database from (Salman et al., 2002) is defined by the number of unbroken

308

particles. To maintain the consistency with the other data source, this is converted by

309

calculation to the breakage probability. In their original source, the breakage ratios are

310

plotted as a function of impact velocity (Jägers et al., 2021; Portnikov et al., 2018; Salman et

311

al., 2002). These experimental results clearly indicate the breakage ratio is varied as function

312

of impact angles irrespective of particle size. The breakage ratios show the maximum value

313

under normal impact angle and then diminish significantly with the decrease of impact angle.

314

3.2 DEM database

315

The DEM database includes the breakage data reported by Moreno et al. 2003 and Ye et al.

316

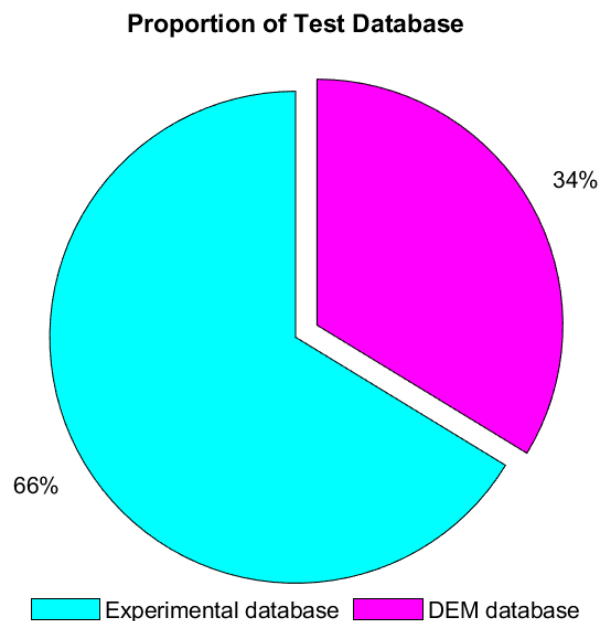
2021. In Moreno et al. 2003, the extent of breakage is characterised by damage ratio, which

317

is defined as the ratio of broken contact numbers to the initial contact numbers (Moreno et

318 al., 2003). The damage ratio is plotted as a function of six impact angles, i.e. 30°, 45°, 60°, 70°,
319 80°, 90° and the impact velocity is varied from 1.15 m/s to 3.41 m/s subject to the six impact
320 angles. The general trend of their study indicates increasing damage ratio with increased
321 impact velocity for the same impact angle. Moreover, the increase of damage ratio is
322 observed when the impact angle is increased from 30° to 90°. The breakage data from (Ye et
323 al., 2021) covers the damage ratio spanning from zero until 0.8, resulted from the impact
324 velocity between 4 m/s to 14 m/s subject to five impact angles, i.e. 15°, 35°, 55°, 75°, and 90°.
325 Similar conclusions were drawn; increase of impact angle resulted in an increased damage
326 ratio for the same impact velocity. In particular, lower impact angles demonstrated a
327 widening gap of damage ratio compared to that under normal impact given the same impact
328 velocity. Figure 4 depicts the proportion of experimental and DEM database amongst the
329 literature database.

330 In view of both experimental and DEM database, it is firmly believed that a wide spectrum of
331 oblique impact is covered in the present study, which is expected to sufficiently satisfy the
332 amount of data for the oblique impact model assessment.



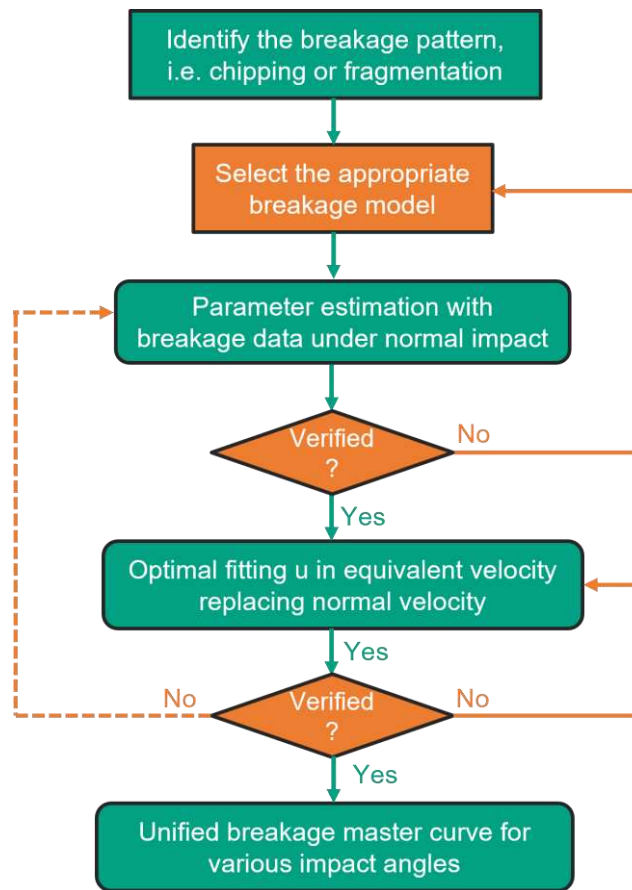
333

334 Figure 4 Proportion of experimental and DEM database in the scoped literature

335 4 Assessment of the oblique impact breakage model

336 4.1 Model assessment procedure

337 The breakage model assessment procedure can be divided as the following steps (shown in
338 Figure 5). The first step is to identify the breakage pattern, i.e. chipping or fragmentation. The
339 second step is to choose the appropriate model expression. A variety of breakage models
340 under normal impact was developed for chipping and fragmentation in the literature. In this
341 stage, mathematical simplicity and physical meaning of model parameters are given priority
342 in the model selection. In this work, the breakage models will be directly selected from the
343 original source of the breakage data. For the original source without specification of breakage
344 models, Vogel and Peukert model is assigned for the test data from (Ye et al., 2021), due to
345 the success of this model in the construction of the unified breakage master curve. The third
346 step is to estimate the fitting parameters in the breakage models against the normal impact
347 breakage data. The fourth step is to adopt the equivalent velocity replacing impact velocity in
348 the breakage models as selected in the second step. The optimal value of friction mobilisation
349 parameter ψ will be achieved against the breakage data under various impact angles.



350

351

Figure 5 Model assessment flowchart for unified breakage master curve

352 4.2 Particle breakage master curve

353 4.2.1 Statistical performance

354 The statistical performance of each model as assessed by the collected data is given in Table
 355 2. Table 2 first shows the normal impact models corresponding to the individual data source,
 356 where the model parameters are fitted with only the normal impact data. Then the fitting
 357 parameter ψ in the proposed oblique impact model is achieved with the oblique impact
 358 breakage dataset. Despite differing normal impact models used for normal impact data fitting,
 359 utilizing the equivalent velocity from the proposed oblique impact model gives rise to ψ^2 . As
 360 only one set of fitting parameters is required for various impact angles in the sourced dataset,
 361 the fitting efficiency is thus significantly improved as compared to individual parameter fitting
 362 subject to every impact angle. For example, there are total 7 impact angles considered in the
 363 dataset from (Jägers et al., 2021). The model fitting efficiency is considerably improved by 86%
 364 using one set of fitting parameters in Table 2, compared to the conventional seven sets of
 365 fitting parameters with regards to the seven impact angles accordingly.

366 Table 2 Fitting parameter and reduced efforts in parameter estimation

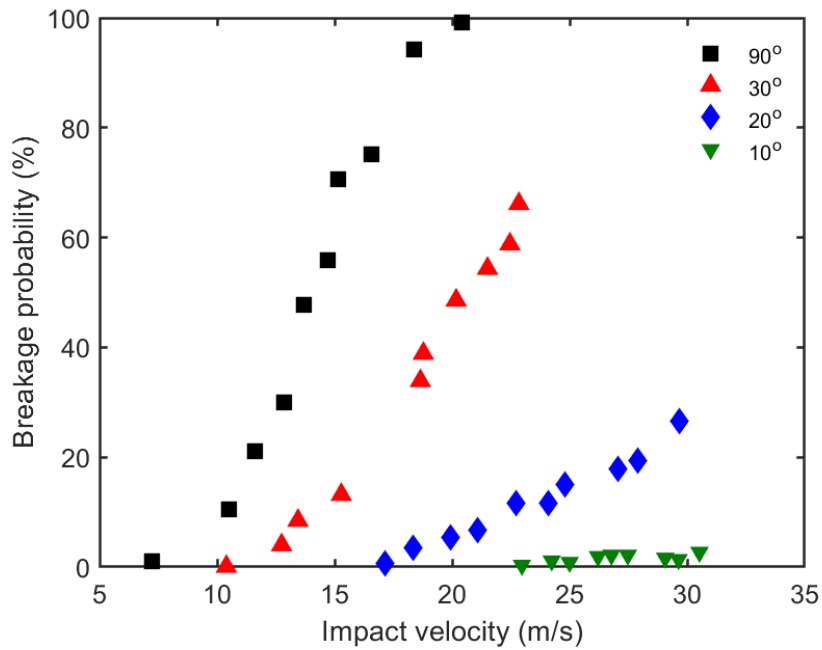
Data source	Normal impact model and fitting parameters	Oblique impact model and fitting parameters	Breakage type	Improved fitting efficiency - (Set of fitting parameters with and without the oblique impact model)	
(Salman et al., 2002)	Salman model		Fragmentation	75% - (1:4)	
	m	15.14			(Wang et al., 2021a) $\psi^2 = 0.89$
	n	5.25			
	R^2	0.995			
(Moreno et al., 2003)	Wang model		Chipping	83% - (1:6)	
	m	0.12			(Wang et al., 2021a) $\psi^2 = 0.031$
	n	1.2			
	R^2	0.995			
(Portnikov et al., 2018)	Portnikov model		Fragmentation	86% - (1:7)	
	v_{50}	11.9			(Wang et al., 2021a) $\psi^2 = 0.39$
	b	2.25			
	R^2	0.995			
(Jägers et al., 2021)	Portnikov model		Fragmentation	86% - (1:7)	
	v_{50}	19.98			(Wang et al., 2021a) $\psi^2 = 0.71$
	b	2.55			
	R^2	0.998			
(Ye et al., 2021)	Vogel and Peukert model		Fragmentation	83% - (1:6)	
	f_{Mat} (kg/Jm)	0.33			(Wang et al., 2021a) $\psi^2 = 1.06$
	$W_{m,min}$ (J/kg)	0.52			
	R^2	0.991			

368 4.2.2 Graphical comparison

369 The predicted breakage probability using the equivalent velocity is compared with the test
370 database to assess the applicability of the proposed oblique impact model in Figures 6, 7, 8,
371 9 and 10. An example of chipping model assessment with the test data from (Moreno et al.,
372 2003) is presented in Figure 7. The breakage data is reasonably assumed to follow a power
373 trend under normal impact. The velocity exponent is determined as 1.2 using the nonlinear
374 least squares method. Whilst keeping the velocity exponent fitted from normal impact
375 constant, the impact velocity is replaced with the equivalent normal velocity to fit the oblique
376 model parameters against the test data from the five impact angles 80° , 70° , 60° , 45° , 30° .
377 In Figure 7a, without the adoption of equivalent velocity proposed in the present work, the
378 breakage probability under various impact angles differs markedly with a large scatter. The
379 principal cause for the scatter is attributed that the contribution of tangential velocity is not
380 considered in majority of existing breakage models. As a stark contrast, Figure 7b clearly
381 shows a unified breakage master curve of chipping database under various impact angles.
382 This is attributed to the equivalent velocity where the contribution from tangential velocity
383 can be rationalized. Taking the fragmentation database from (Jägers et al., 2021) as another
384 example, the breakage ratio predicted using the equivalent velocity are compared with the
385 test results in Figure 9. Figure 9a is the plot of reported breakage probability of wood pellet
386 with particle length 15 mm in dataset 2 and Figure 9b is the predicted breakage probability
387 by equivalent normal velocity under seven impact angles, 90° , 70° , 50° , 45° , 40° , 30° , 20° .

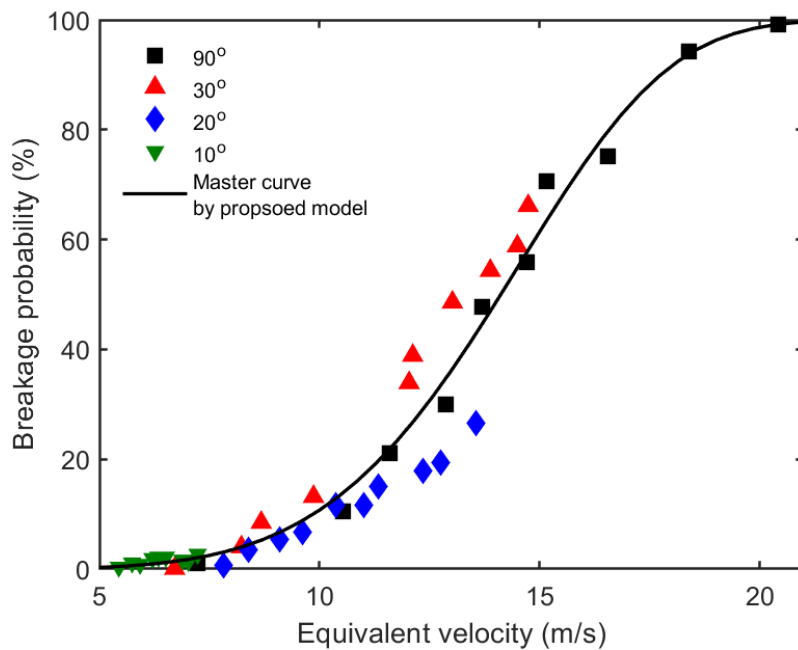
388 In Figure 9a, the breakage probability of wood pellets at seven impact angles are nearly the
389 same at the impact velocity 5 m/s. When the impact velocity is increased as 15 m/s, the
390 breakage rate under oblique impact becomes more scattered as a function of impact angles.
391 In particular, the breakage probability is increased with the increase of impact angle and the
392 scatter of breakage probability under oblique impact is widening with higher impact velocity
393 until 40 m/s. The breakage dataset from (Jägers et al., 2021) clearly indicates a fragmentation
394 mechanism and hence Portnikov et model is appropriately used for the parameter fitting
395 under normal impact. Following the model assessment procedure, Figure 9b displays a unified
396 breakage master curve as a function of equivalent velocity. Likewise, the unified breakage
397 master curves using the equivalent velocity in Eq. (19) are also observed in Figures 5, 7, and 9
398 for the breakage data from (Portnikov et al., 2018; Salman et al., 2002; Ye et al., 2021). The

399 predicted and surveyed breakage probabilities by means of equivalent velocity and literature
400 database respectively, are depicted in Figure 11. This parity plot displays the surveyed test
401 data on the horizontal axis and predicted values on the vertical axis. This again indicates a
402 strong predictive accuracy from the oblique impact model where the total 175 data points
403 follows the diagonally linear (1:1) line.



404
405

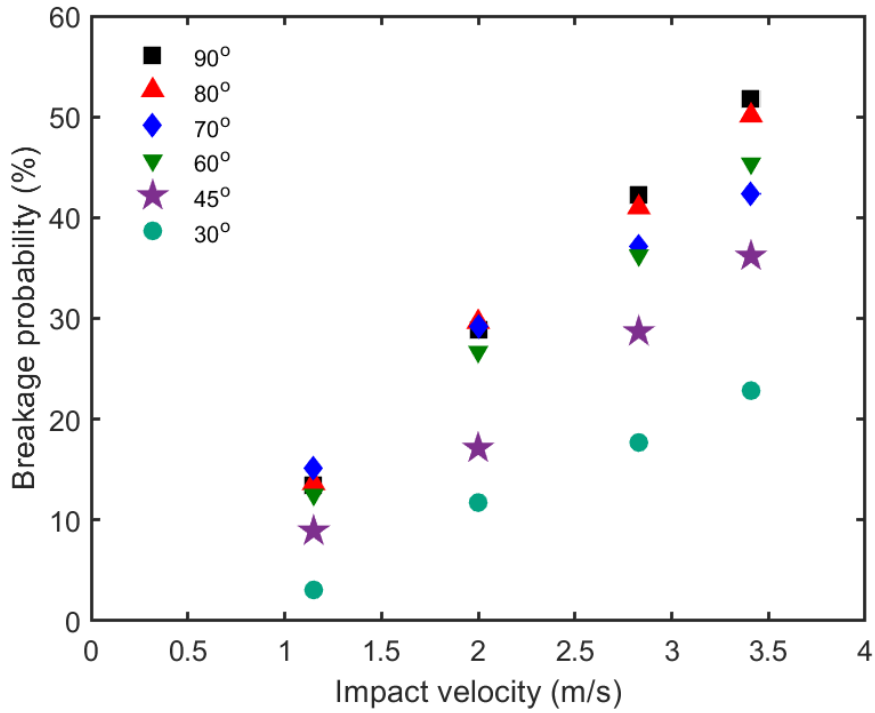
(a)



406
407

(b)

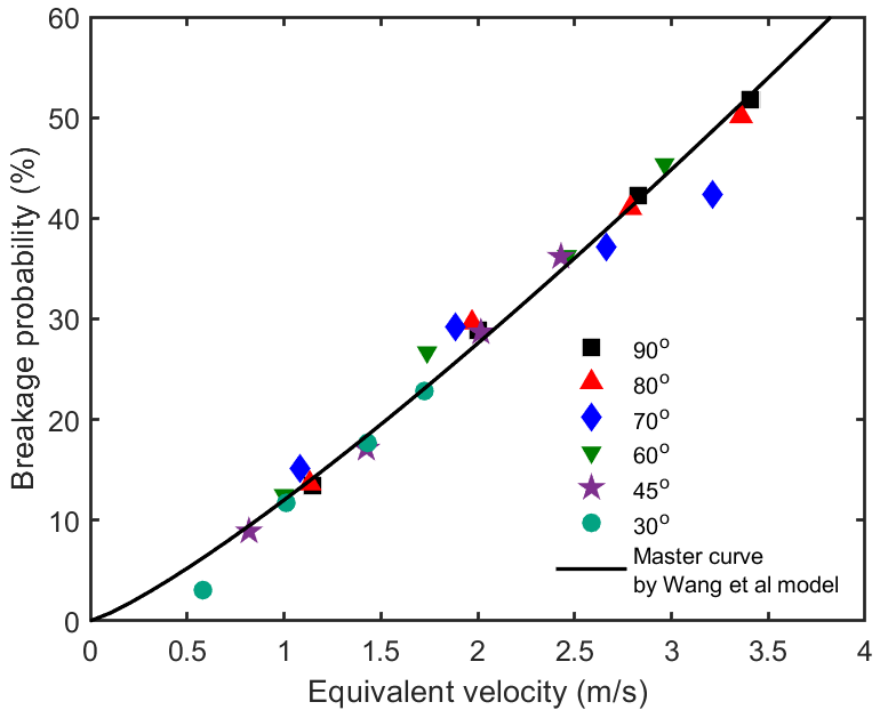
408 Figure 6 (a) Breakage database from Salman et al. 2002 versus (b) master curve using
409 proposed oblique impact model



410

411

(a)

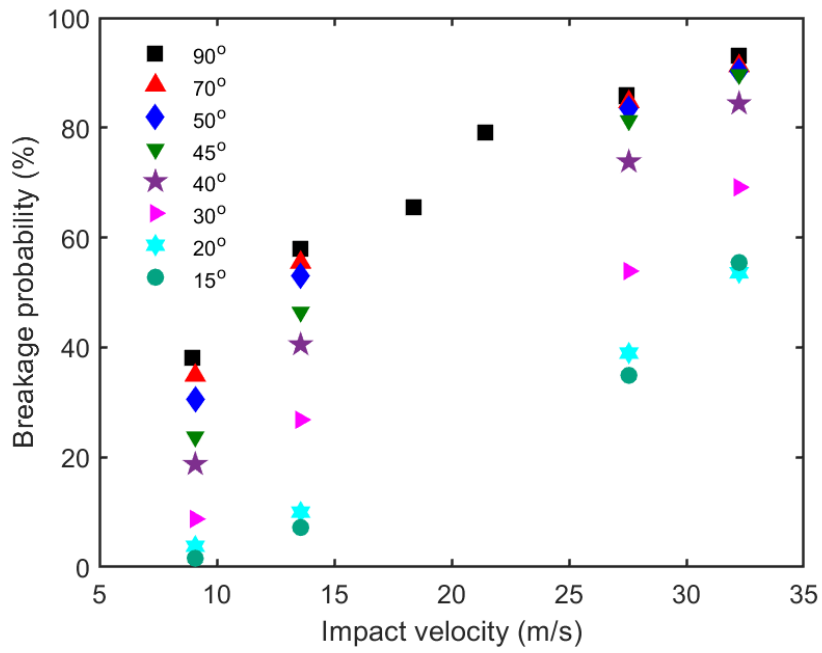


412

413

(b)

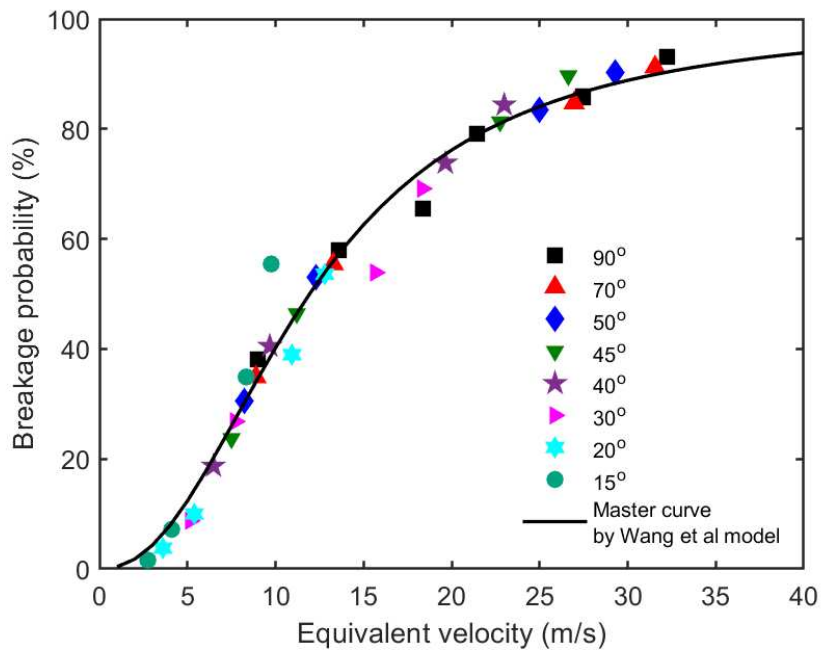
414 Figure 7 (a) Breakage database from Moreno et al. 2003 versus (b) master curve using
415 proposed oblique impact model



416

417

(a)

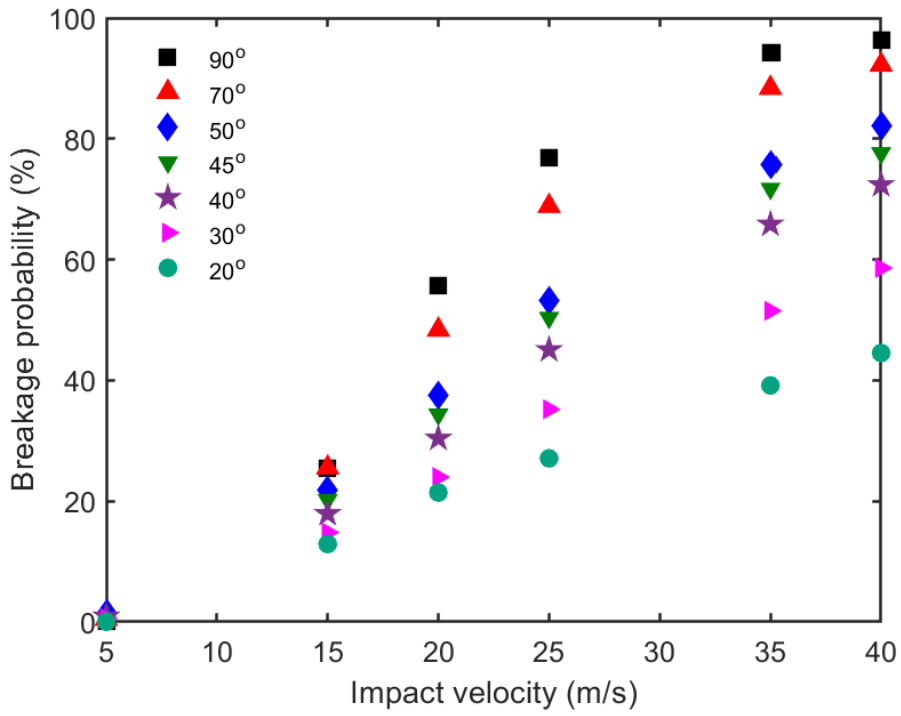


418

419

(b)

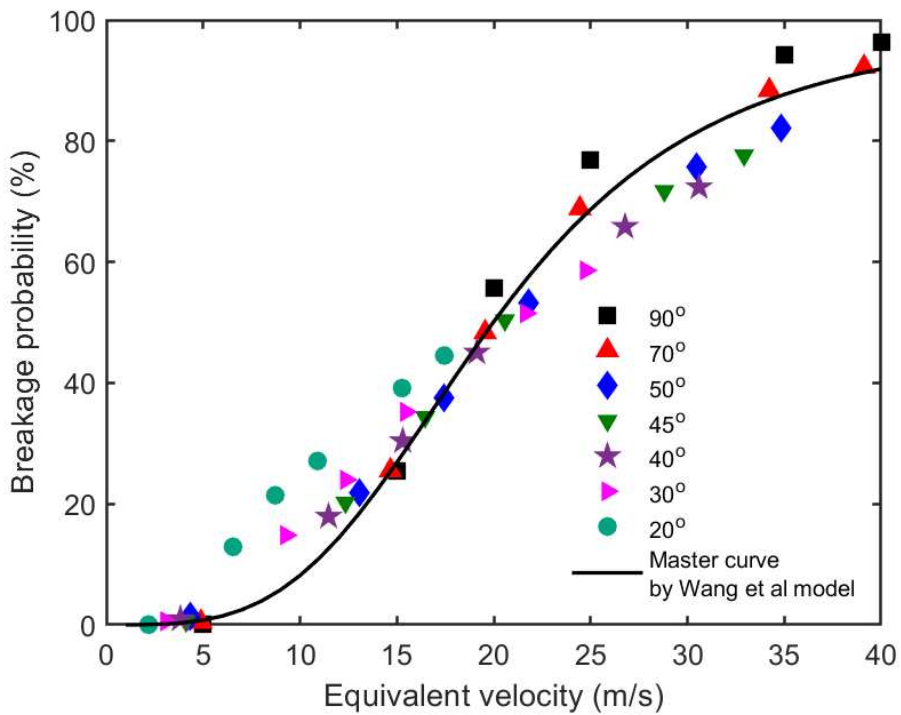
420 Figure 8 (a) Breakage database from Portnikov et al. 2018 versus (b) master curve using
421 proposed oblique impact model



422

423

(a)



424

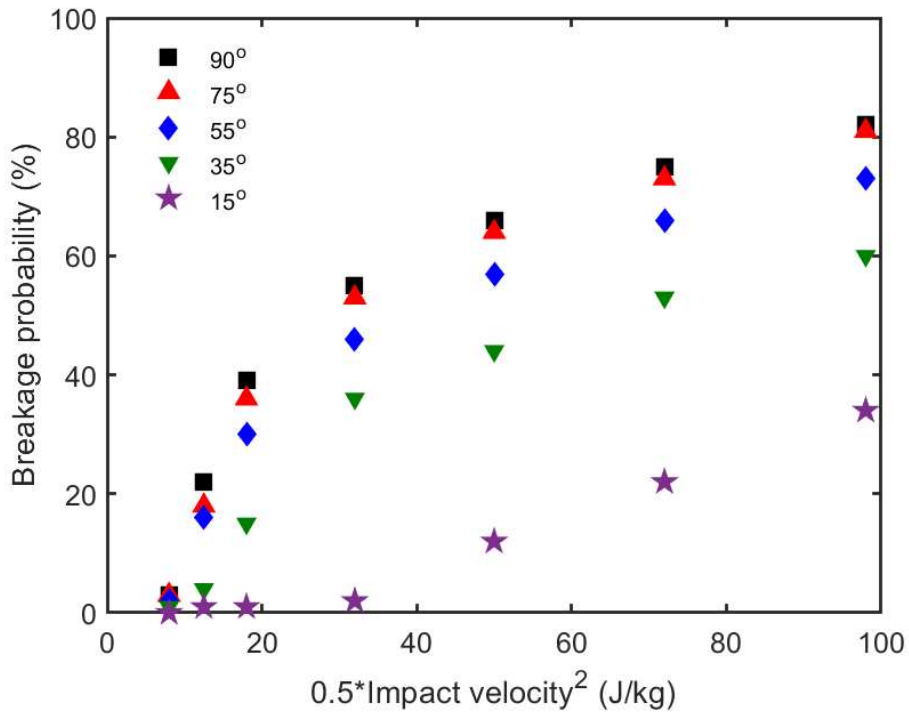
425

(b)

426

427

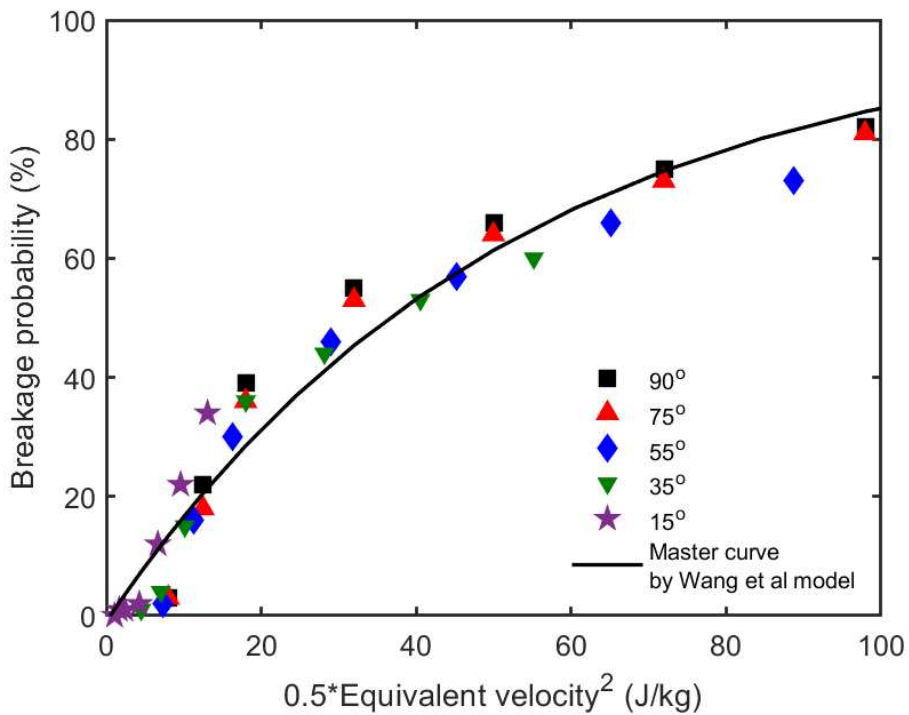
Figure 9 (a) Breakage database from Jägers et al. 2021 versus (b) master curve using proposed oblique impact model



428

429

(a)



430

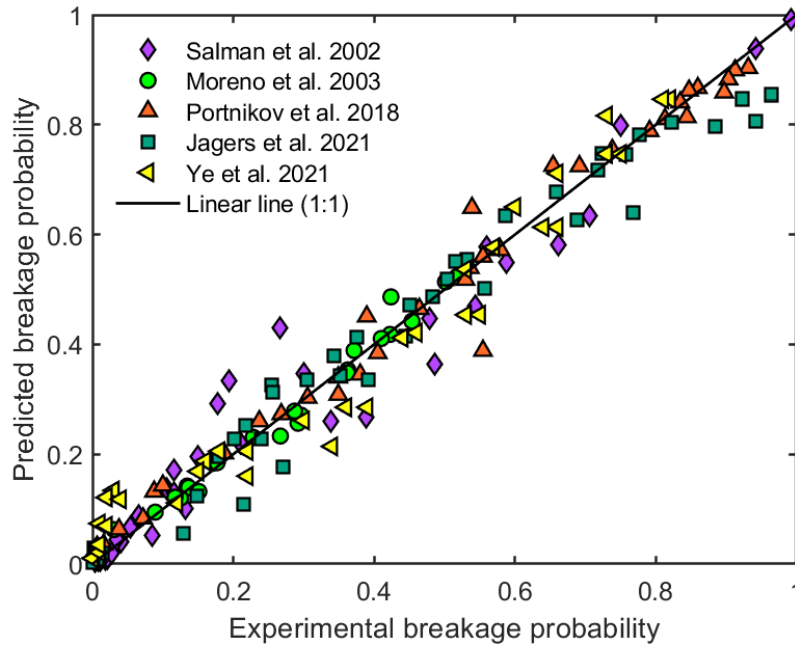
431

(b)

432 Figure 10 (a) Breakage database from Ye et al. 2021 versus (b) master curve using proposed

433

oblique impact model



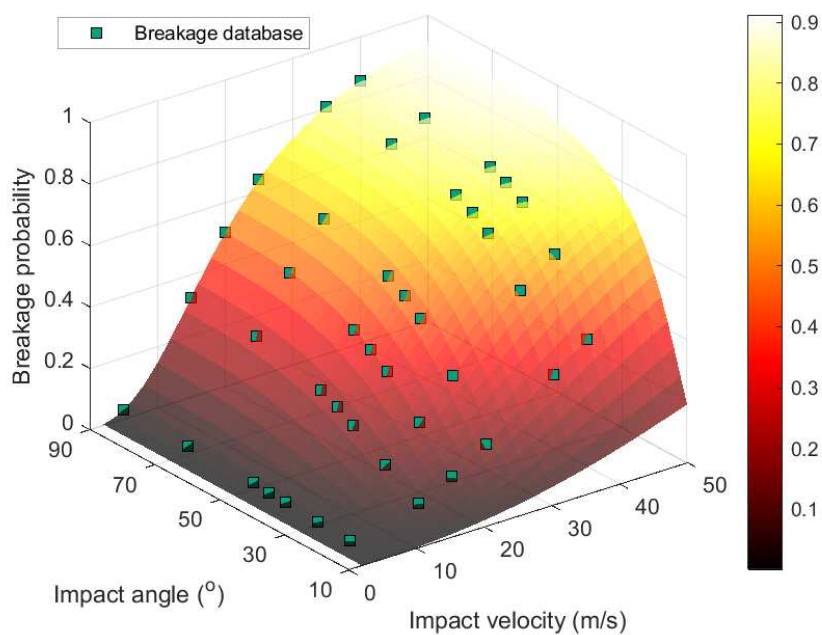
434

435 Figure 11 Experimental vs predicted breakage probability for all the breakage database

436 **4.3 Discussion**

437 Results from the oblique impact model assessment clearly show the universality of the
 438 proposed equivalent velocity in unifying the master curves with all the deployed test data.
 439 Compared to the conventional experimental studies, the proposed oblique impact model
 440 provides a theoretical solution for oblique impact conditions. Significant improvement of
 441 breakage probability prediction can be made by only one set of fitting parameters for various
 442 impact angles. A mapping regime of breakage probability subject to oblique impact can thus
 443 be readily established with the calibrated parameters setup. For instance, with the calibrated
 444 parameters against the dataset from (Jägers et al., 2021), the breakage probability map based
 445 on Portnikov et al. model is plotted in Figure 12 where the contribution of both impact
 446 velocity and impact angle can be quantified. In the preceding study any further attempts of
 447 oblique impact breakage beyond the test data have to be experimentally performed as
 448 hindsight. As shown in Figure 12, the proposed oblique impact model is capable of predicting
 449 breakage probability with consideration of both impact velocity and impact angle. The oblique
 450 impact model is also promising for coupling DEM with other computational techniques such
 451 as computational fluid dynamics (CFD) or population balance model (PBM). Despite the
 452 insights of particle collision information from DEM, the critical information such as the
 453 distribution of impact angle and its role in the multiphase interaction has not yet been

454 effectively explored. The issue regarding inadequacy or ignorance of impact angle in DEM-
455 CFD or DEM-PBM coupling will be especially significant where the oblique impact in the
456 particulate processes such as fluid bed granulation and dry milling is frequent. Another
457 challenge remains whether the proposed equivalent velocity in the oblique impact model can
458 be used to unify the breakage function, i.e. fragment size distribution with respect to varying
459 impact angles. This forms a potential research topic for further work, to examine whether a
460 unified curve of particle size distribution can be similarly constructed given varying impact
461 angles.



462
463 Figure 12 Breakage mapping regime created using the proposed oblique impact model
464 based on the database from (Jägers et al., 2021)

465 5 Conclusions

466 This paper has presented a simple and effective oblique impact model where the breakage
467 master curve can be invariably established for various impact angles. The motivation behind
468 this developed model is driven by the omission of tangential velocity component in the
469 conventional breakage models. The breakage probability is likely to be underestimated when
470 calculated considering only from the normal velocity component, ignoring the tangential
471 velocity component. The novelty of the proposed model lies in the consideration of tangential

472 velocity component, the physical consideration of friction coefficient, and most importantly
473 a unified breakage master curve using the paradigm of equivalent velocity.

474 The assessment of breakage models under oblique impact was conducted using the collected
475 breakage database from the literature. The developed oblique impact model is shown to be
476 generally applicable in all the oblique impact circumstances. This is the first oblique impact
477 model where the breakage probability subject for oblique impacts can be unified with a master
478 curve, overcoming the experimental limitations and considerably improving the fitting
479 efficiency and predictive accuracy. The developed oblique impact model is therefore
480 recommended for future exploration of particle dynamics, where oblique impacts are
481 significant. It is expected this model will be of particular use in future DEM-CFD or DEM-PBM
482 coupling scenarios.

483 **Nomenclature**

a	Fitting parameter, -
A_v	Fitting parameter, -
b	Fitting parameter in Eqs. (2) and (4), -
c	Fitting parameter, -
d	Particle diameter in Eq. (1), mm
d_0	Fitting parameters, -
e	Fraction of loss energy in Eq. (6), -
a, b, c, d, e	Exponent in Eq. (10), -
E	Mass specific energy, J/kg
$E_{50,i}$	Median mass specific energy, J/kg
E_{loss}	Mass-specific collision energy, J/kg
E'_{loss}	Total energy loss in the collision, J/kg
f_{Mat}	Resistance of the particle against the external stressing, $\text{kgJ}^{-1}\text{m}^{-1}$
F	Impact force, N
F_n	Normal impact force, N
F_t	Tangential impact force, N
F_e	Equivalent impact force, N
H	Particle hardness, GPa

k	Hertzian stiffness of the contact target, -
k_c	Fracture toughness, MPa.m ^{1/2}
m_p	Mass of a pellet, g
m	A single lumping parameter, -
n	Impact number in Eq. (9), -
P_E	Breakage probability as a function of specific energy, -
P	Breakage probability, selection function, -
P_x	Breakage probability, -
t_{10}	Breakage index (%), -
v	Impact velocity, -
v_n	Normal component of impact velocity, -
v_t	Tangential component of impact velocity, -
v_{50}	Median impact velocity resulting in 50% of particle breakage, m/s
v_e	Equivalent velocity, -
W_m	The mass-specific energy, -
$W_{m,min}$	Mass-specific threshold energy for particle to break, -
$W_{m,kin}$	Mass-specific kinetic energy, -
x	Particle size, -
z	Fitting parameter, -

484 **Greek symbols**

σ	Standard deviation of the specific energy, J/kg
θ	Impact angle, °
ρ	Particle density, kg/m ³
α	Fitting parameter, -
μ	Dynamic friction coefficient, -

485

486 **Appendix**

487 Table A1 Features of test conditions from the literature breakage database

Database No.	Source literature	Source data	Test particle and diameter	Test method	Breakage pattern	Amount of data
1	(Salman et al., 2002)	Figure 4	Fertiliser particle, 3.2 mm	Experimental Horizontal impact	Fragmentation	40
2	(Moreno et al., 2003)	Figure 3	Agglomerate, 1.814 mm	DEM	Chipping	24
3	(Portnikov et al., 2018)	Figure 4	Salt particle, 2.36-3.35 mm	Experimental Horizontal impact	Fragmentation	34
4	(Jägers et al., 2021)	Figure 6b	Wood pellet, 15 mm	Experimental Horizontal impact	Fragmentation	42
5	(Ye et al., 2021)	Figure 12a	Marble sphere, 58 mm	DEM	Fragmentation	35

488

489 **Acknowledgement**

490 The writers gratefully acknowledge the financial support from Innovate UK for the Knowledge
491 Transfer Partnership Grant No. 158229 between The University of Sheffield and Process
492 Systems Enterprise.

493 **References**

494 Andrews, E.W., Kim, K.S., 1999. Threshold conditions for dynamic fragmentation of glass
495 particles. *Mech. Mater.* 31, 689–703. [https://doi.org/10.1016/S0167-6636\(99\)00024-1](https://doi.org/10.1016/S0167-6636(99)00024-1)

496 Antonyuk, S., Khanal, M., Tomas, J., Heinrich, S., Mörl, L., 2006. Impact breakage of spherical
497 granules: Experimental study and DEM simulation. *Chem. Eng. Process. Process Intensif.*
498 45, 838–856. <https://doi.org/10.1016/j.cep.2005.12.005>

499 Boerefijn, R., Gudde, N.J., Ghadiri, M., 2000. Review of attrition of fluid cracking catalyst
500 particles. *Adv. Powder Technol.* 11, 145–174.
501 <https://doi.org/10.1163/156855200750172286>

502 Bwalya, M., Chimwani, N., 2020. Development of a More Descriptive Particle Breakage
503 Probability Model 10, 710.

504 Cavalcanti, P.P.S., Petit, H.A., Thomazini, A.D., de Carvalho, R.M., Tavares, L.M., 2021.
505 Modeling of degradation by impact of individual iron ore pellets. *Powder Technol.* 378,
506 795–807. <https://doi.org/10.1016/j.powtec.2020.10.037>

507 Chen, X., Wang, L.G., Morrissey, J.P., Ooi, J.Y., 2022. DEM simulations of agglomerates impact
508 breakage using Timoshenko beam bond model. *Granul. Matter* 24.
509 <https://doi.org/10.1007/s10035-022-01231-9>

510 Cheong, Y.S., Salman, A.D., Hounslow, M.J., 2003. Effect of impact angle and velocity on the
511 fragment size distribution of glass spheres. *Powder Technol.* 138, 189–200.
512 <https://doi.org/10.1016/j.powtec.2003.09.010>

513 Cleaver, J.A.S., Ghadiri, M., Rolfe, N., 1993. Impact attrition of sodium carbonate
514 monohydrate crystals. *Powder Technol.* 76, 15–22. [https://doi.org/10.1016/0032-
515 5910\(93\)80036-A](https://doi.org/10.1016/0032-5910(93)80036-A)

516 De Carvalho, R.M., Tavares, L.M., 2013. Predicting the effect of operating and design variables

517 on breakage rates using the mechanistic ball mill model. *Miner. Eng.* 43–44, 91–101.
518 <https://doi.org/10.1016/j.mineng.2012.09.008>

519 Duo, W., Boerefijn, R., Ghadiri, M., 1996. Impact attrition of fluid cracking catalyst, in:
520 Proceedings of 5th International Conference on Multiphase Flow in Industrial Plants. pp.
521 170–179.

522 Evans, A.G., Gulden, M.E., Rosenblatt, M., 1978. Impact Damage in Brittle Materials in the
523 Elastic-Plastic Response Regime. *Proc. R. Soc. A Math. Phys. Eng. Sci.* 361, 343–365.
524 <https://doi.org/10.1098/rspa.1978.0106>

525 Evans, A.G., Wilshaw, T.R., 1976. Quasi-static solid particle damage in brittle solids -- I.
526 Observations, analysis and implications. *Acta Metall.* 24, 939–956.
527 [https://doi.org/doi.org/10.1016/0001-6160\(76\)90042-0](https://doi.org/doi.org/10.1016/0001-6160(76)90042-0)

528 Ge, R., Wang, L., Zhou, Z., 2019. DEM analysis of compression breakage of 3D printed
529 agglomerates with different structures. *Powder Technol.* 356, 1045–1058.
530 <https://doi.org/10.1016/j.powtec.2019.08.113>

531 Ghadiri, M., Zhang, Z., 2002. Impact attrition of particulate solids. Part 1: A theoretical model
532 of chipping. *Chem. Eng. Sci.* 57, 3659–3669. [https://doi.org/10.1016/S0009-](https://doi.org/10.1016/S0009-2509(02)00240-3)
533 [2509\(02\)00240-3](https://doi.org/10.1016/S0009-2509(02)00240-3)

534 Jägers, J., Spatz, P., Wirtz, S., Scherer, V., 2021. Analysis of wood pellet degradation
535 characteristics based on single particle impact tests. *Powder Technol.* 378, 704–715.
536 <https://doi.org/10.1016/j.powtec.2020.10.017>

537 Kotzur, B.A., Berry, R.J., Zigan, S., García-Triñanes, P., Bradley, M.S.A., 2018. Particle attrition
538 mechanisms, their characterisation, and application to horizontal lean phase pneumatic
539 conveying systems: A review. *Powder Technol.* 334, 76–105.
540 <https://doi.org/10.1016/j.powtec.2018.04.047>

541 Lawn, B.R., Marshall, D.B., 1979. Hardness, toughness and brittleness, an indentation analysis.
542 *J. Am. Ceram. Soc.* 62, 347–350.

543 Li, Z.P., Wang, L.G., Chen, W., Chen, X., Liu, C., Yang, D., 2020. Scale-up Procedure of
544 Parameter Estimation in Selection and Breakage Functions for Impact pin Milling. *Adv.*
545 *Powder Technol.* 31, 3507–3520.

546 Liu, L., Kafui, K.D., Thornton, C., 2010. Impact breakage of spherical, cuboidal and cylindrical
547 agglomerates. Powder Technol. 199, 189–196.
548 <https://doi.org/10.1016/j.powtec.2010.01.007>

549 Meier, M., John, E., Wieckhusen, D., Wirth, W., Peukert, W., 2009. Influence of mechanical
550 properties on impact fracture: Prediction of the milling behaviour of pharmaceutical
551 powders by nanoindentation. Powder Technol. 188, 301–313.
552 <https://doi.org/http://dx.doi.org/10.1016/j.powtec.2008.05.009>

553 Moreno-Atanasio, R., Ghadiri, M., 2006. Mechanistic analysis and computer simulation of
554 impact breakage of agglomerates: Effect of surface energy. Chem. Eng. Sci. 61, 2476–
555 2481. <https://doi.org/10.1016/j.ces.2005.11.019>

556 Moreno, R., Ghadiri, M., Antony, S.J., 2003. Effect of the impact angle on the breakage of
557 agglomerates: A numerical study using DEM. Powder Technol. 130, 132–137.
558 [https://doi.org/10.1016/S0032-5910\(02\)00256-5](https://doi.org/10.1016/S0032-5910(02)00256-5)

559 Mueller, P., Aman, S., Tomas, J., 2014. Evaluation of impact velocity and compression force of
560 moist zeolite 4A granules at breakage using an equivalence function. Chem. Eng. Technol.
561 37, 813–818. <https://doi.org/10.1002/ceat.201300792>

562 Mueller, P., Antonyuk, S., Stasiak, M., Tomas, J., Heinrich, S., 2011. The normal and oblique
563 impact of three types of wet granules. Granul. Matter 13, 455–463.
564 <https://doi.org/10.1007/s10035-011-0256-5>

565 Petukhov, Y., Kalman, H., 2004. Empirical breakage ratio of particles due to impact. Powder
566 Technol. 143–144, 160–169. <https://doi.org/10.1016/j.powtec.2004.04.009>

567 Pocock, J., Veasey, T.J., Tavares, L.M., King, R.P., 1998. The effect of heating and quenching
568 on grinding characteristics of quartzite. Powder Technol. 95, 137–142.
569 [https://doi.org/10.1016/S0032-5910\(97\)03333-0](https://doi.org/10.1016/S0032-5910(97)03333-0)

570 Portnikov, D., Peisakhov, R., Gabrieli, G.O., Kalman, H., 2018. Selection function of particles
571 under impact loads: The effect of collision angle. Part. Sci. Technol. 36, 420–426.
572 <https://doi.org/10.1080/02726351.2017.1346022>

573 Rozenblat, Y., Grant, E., Levy, A., Kalman, H., Tomas, J., 2012. Selection and breakage
574 functions of particles under impact loads. Chem. Eng. Sci. 71, 56–66.

575 <https://doi.org/10.1016/j.ces.2011.12.012>

576 Rozenblat, Y., Levy, A., Kalman, H., Peyron, I., Ricard, F., 2013. A model for particle fatigue due
577 to impact loads. *Powder Technol.* 239, 199–207.
578 <https://doi.org/10.1016/j.powtec.2013.01.059>

579 Salman, A., Fu, J., Gorham, D., Hounslow, M., 2003. Impact breakage of fertiliser granules.
580 *Powder Technol.* 130, 359–366. [https://doi.org/10.1016/S0032-5910\(02\)00237-1](https://doi.org/10.1016/S0032-5910(02)00237-1)

581 Salman, A.D., Fu, J., Gorham, D.A., Hounslow, M.J., 2003. Impact breakage of fertiliser
582 granules. *Powder Technol.* 130, 359–366. [https://doi.org/10.1016/S0032-](https://doi.org/10.1016/S0032-5910(02)00237-1)
583 [5910\(02\)00237-1](https://doi.org/10.1016/S0032-5910(02)00237-1)

584 Salman, A.D., Gorham, D.A., Verba, A., 1995. A study of solid particle failure under normal and
585 oblique impact. *Wear* 186–187, 92–98. [https://doi.org/10.1016/0043-1648\(95\)07140-7](https://doi.org/10.1016/0043-1648(95)07140-7)

586 Salman, A.D., Hounslow, M.J., Verba, A., 2002. Particle fragmentation in dilute phase
587 pneumatic conveying. *Powder Technol.* 126, 109–115. [https://doi.org/10.1016/S0032-](https://doi.org/10.1016/S0032-5910(02)00048-7)
588 [5910\(02\)00048-7](https://doi.org/10.1016/S0032-5910(02)00048-7)

589 Shi, F., 2016. A review of the applications of the JK size-dependent breakage model: Part 1:
590 Ore and coal breakage characterisation. *Int. J. Miner. Process.* 155, 118–129.
591 <https://doi.org/10.1016/j.minpro.2016.08.012>

592 Subero, J., Ghadiri, M., 2001. Breakage patterns of agglomerates. *Powder Technol.* 120, 232–
593 243. [https://doi.org/10.1016/S0032-5910\(01\)00276-5](https://doi.org/10.1016/S0032-5910(01)00276-5)

594 Tavares, L.M., 2021. Review and Further Validation of a Practical Single-particle Breakage
595 Model † 1–22.

596 Tavares, L.M., 2009. Analysis of particle fracture by repeated stressing as damage
597 accumulation. *Powder Technol.* 190, 327–339.
598 <https://doi.org/10.1016/j.powtec.2008.08.011>

599 Tavares, L.M., 2004. Optimum routes for particle breakage by impact. *Powder Technol.* 142,
600 81–91. <https://doi.org/10.1016/j.powtec.2004.03.014>

601 Tavares, L.M., King, R.P., 1998. Single-particle fracture under impact loading. *Int. J. Miner.*
602 *Process.* 54, 1–28. [https://doi.org/10.1016/S0301-7516\(98\)00005-2](https://doi.org/10.1016/S0301-7516(98)00005-2)

603 Vogel, L., Peukert, W., 2003. Breakage behaviour of different materials - Construction of a
604 mastercurve for the breakage probability. *Powder Technol.* 129, 101–110.
605 [https://doi.org/10.1016/S0032-5910\(02\)00217-6](https://doi.org/10.1016/S0032-5910(02)00217-6)

606 Wang, L.G., 2016. Particle Breakage Mechanics in Milling Operation. University of Edinburgh.

607 Wang, L.G., Chen, J.-F., Ooi, J.Y., 2021a. A breakage model for particulate solids under impact
608 loading. *Powder Technol.* 394, 669–684. <https://doi.org/10.1016/j.powtec.2021.08.056>

609 Wang, L.G., Ge, R., Chen, X., 2022. Establishing an oblique impact breakage master curve using
610 a DEM bonded contact model. *Comput. Geotech.* 145, 104668.
611 <https://doi.org/10.1016/j.compgeo.2022.104668>

612 Wang, L.G., Ge, R., Chen, X., 2021b. On the determination of particle impact breakage in
613 selection function. *Particuology*. <https://doi.org/10.1016/j.partic.2021.08.003>

614 Wang, L.G., Ge, R., Chen, X., Zhou, R., Chen, H.M., 2021c. Multiscale digital twin for particle
615 breakage in milling: From nanoindentation to population balance model. *Powder
616 Technol.* 386, 247–261. <https://doi.org/10.1016/j.powtec.2021.03.005>

617 Wang, L.G., Li, Z.P., Zhang, L.Z., Zhou, R.X., Chen, X.Z., 2021d. On the Measurement of Particle
618 Contact Curvature and Young's Modulus Using X-ray μ CT. *Appl. Sci.* 11.

619 Wang, L.G., Ooi, J.Y., Butler, I., 2015. Interpretation of particle breakage under compression
620 using X-ray computed tomography and digital image correlation, in: *Procedia
621 Engineering*. <https://doi.org/10.1016/j.proeng.2015.01.138>

622 Ye, Y., Zeng, Y., Cheng, S., Sun, H., Chen, X., 2021. Computers and Geotechnics Numerical
623 investigation of rock sphere breakage upon oblique impact : effect of the contact friction
624 coefficient and impact angle. *Comput. Geotech.* 136, 104207.
625 <https://doi.org/10.1016/j.compgeo.2021.104207>

626 Zhang, L.Z., Wang, L.G., Wang, Y., He, Y., Chen, X., 2022. Validation of a particle impact
627 breakage model incorporating impact number effect. *Particuology Pre-proof*.